Rock and Soil Mechanics

Volume 43 | Issue 5 Article 2

7-4-2022

Shear strength deterioration of geopolymer stabilized loess under wet-dry cycles: mechanisms and prediction model

Rui CHEN

Xing ZHANG

Ruo-yu HAO

Wei-xing BAO

Custom Citation

CHEN Rui, ZHANG Xing, HAO Ruo-yu, BAO Wei-xing. Shear strength deterioration of geopolymer stabilized loess under wet-dry cycles: mechanisms and prediction model[J]. Rock and Soil Mechanics, 2022, 43(5): 1164-1174.

Rock and Soil Mechanics 2022 43(5): 1164−1174 ISSN 1000−7598
https: //doi.org/10.16285/j.rsm.2021.6355 rocksoilmech.researchcommons.org/journal

Shear strength deterioration of geopolymer stabilized loess under wet-dry cycles: mechanisms and prediction model

CHEN Rui, ZHANG Xing, HAO Ruo-yu, BAO Wei-xing
School of Highway, Chang'an University, Xi'an, Shaanxi 710064, China

Abstract: The loess was stabilized using geopolymer (GP). Triaxial compression tests were conducted on stabilized loess with varied GP contents subjected to wet–dry cycles. The degradation law of the shear strength of the stabilized loess after varied wet–dry cycles was evaluated and an empirical model for predicting the shear strength was proposed. The chemical composition of the hydration products, the microstructure and pore size distribution of stabilized loess were investigated by X-ray diffraction (XRD), scanning electron microscopy (SEM) and mercury intrusion porosimetry (MIP) tests. The degradation mechanisms of GP stabilized loess under wet–dry cycles were discussed based on the experimental results. The experimental results show that compared with untreated soil, the shear strength of stabilized soils is significantly improved with the increasing GP content, i.e. the cohesion and internal friction angle increase by 260% and 43%, respectively. The shear strength of stabilized loess decreases with the increasing ratio of porosity to GP volumetric fraction (η / G_{v}) in a power function. It indicates that GP stabilization can remarkably improve the durability of loess under wet–dry cycles. The stabilized loess with 10% and 15% GP can maintain over 75% of their original shear strength, but those with 5% GP shows evident deterioration in shear strength after nine wet–dry cycles. The wet–dry cycling has greater impact on the degradation of peak deviatoric stress and cohesion than that of internal friction angle. An empirical model was proposed and validated for predicting the degradation in shear strength of the GP stabilized loess under wet–dry cycles, considering influence of the GP content, confining pressure and the number of wet–dry cycle. The experimental results of XRD, SEM and MIP show that the main hydration products of GP are calcium silicate hydrate (CSH) and calcium aluminosilicate hydrate (CASH), which fill the soil pores and enhance the bonding between soil particles. Due to this reason, a denser microstructure develops and the cohesion of the stabilized loess increases, which consequently improves the shear strength of the GP stabilized loesses. Moreover, the wet–dry cycle results in the expansion of soil pores and the formation of new fissures, which destructs the bonding between soil particles and reduces the shear strength of the stabilized loess.

Keywords: loess; geopolymer; wet–dry cycle; shear strength deterioration; stabilizing mechanism; prediction model

1 Introduction

Extensive loess deposits are found in northwestern China. Loess processes large pores and a metastable structure which is sensitive to the change in water content. The vertical cracks are commonly observed in the natural loess. Particularly, the structure would be broken down, and even an immediate, considerable and non-uniform collapse could occur when the loess is saturated. The collapsible characteristics of loess pose many challenges for construction[1]. Therefore, it is of significance to stabilize the collapsible loess to meet the requirements of construction sites which are located in collapsible loess strata. The treatment of the loess with the stabilizer, such as cement, lime and fly ash, has been widely used for the loess stabilization.

In the context of soil–atmosphere interaction, the cyclic environmental loading due to rainfall infiltration and evaporation generally results in the deterioration of the mechanical properties and engineering performance of the stabilized loess. The evaluation of the durability of the stabilized loess subjected to wet–dry cycles has been paid extensive attention in engineering practice. To date, numerous studies have been devoted to investigating the deterioration of the mechanical properties of the stabilized loess due to the effect of wet–dry cycles. Jiang et al.[2] found that the strength of the cement stabilized loess increased linearly with the increase of the content of cement, which reached a stable value after 15 wet–dry cycles. Zhong et al.[3] conducted dynamic triaxial tests on the fly ash stabilized loess specimens after wet–dry cycles. They found that the dynamic strength of the stabilized loess increased remarkably than the untreated loess and the critical dynamic stress of the stabilized loess decreased due to the wet–dry cycles Ji et al.[4] found that the shear strength of the loess stabilized by the compound (i.e. fiber, straw ash and lime) decreased as the number of wert–dry cycles increases. The improvement in the strength and durability of the stabilized loess was observed as the curing time increased. The findings in the existing literature on the influence of the number of wet–dry cycles and the type and content of stabilizers on the deterioration in the mechanical properties of the stabilized loess has improved the understanding of the durability of the stabilized loess.

Geopolymer (GP) is a new binder material formed by alkaline activation of aluminosilicate material through chemical reactions, such as dissolution, diffusion, condensation and crystallization to hardening. Clays

Received: 16 August 2021 Revised: 22 October 2021
This work was supported by the National Natural Science Foundation of China (51708041), the Natural Science Foundation of Shaanxi Province (2018JQ5001) and the Fundamental Research Funds for the Central Universities, Chang'an University (300102210213).
First author: CHEN Rui, male, born in 1987, PhD, Associate Professor, mainly engaged in research on special soil mechanical properties and ground treatment. E-mail: rchenua@chd.edu.cn

and metakaolin were widely used as the precursor of geopolymer[5–7]. It was found later that the industrial wastes including steel slag, fly ash, ground granulated blast-furnace slag, calcium carbide slag, could be used as the raw material of geopolymer. Research has revealed that geopolymer has high binding strength, good acid and alkaline resistance, and good high temperature resistance. In addition, the geopolymer could be synthesized from a variety of solid wastes. Therefore, the use of geopolymer contributes the reduced energy consumption and carbon emission, which renders the geopolymer as an excellent alternative to the cement for soil stabilization[8]. Due to this reason, attentions have been drawn to the use of geopolymer as a binder material for soil stabilization recently. Liu et al.[9] and Cristelo et al.[10–13] found that the fly ash-based geopolymer could promote a compact microstructure and improve the strength of the stabilized loess and soft soil. Qiao[14] investigated the strength characteristics of the stabilized loess by the alkali-activated (i.e. sodium hydroxide and calcium hydroxide) industrial waste compound and that by the cement. It was found that the stabilized soil gained a relative low strength at the beginning of the curing process and a remarkable improvement in the strength after a long period of the curing process. In addition, the fly ash content and the initial water content had been found to have a significant influence on the strength of the stabilized loess. Deng et al.[15] found that the addition of 20% alkali–activated steel slag–based geopolymer could remarkably improve the unconfined compression strength of the stabilized soft soil. The microstructure test results indicated that the mesh-shaped calcium silicate hydrate formed, which reduce the pore space between soil particles. Wu et al.[16] investigated the unconfined compression strength of the stabilized muddy clay using the combined slag and fly ash–based geopolymer. They found that the improvement in the strength of the stabilized clay was mainly attributed to the formation of the hydration products, i.e. calcium–silicate–hydrate (CSH) and calcium–aluminosilicate–hydrate (CASH).

The durability of the stabilized loess has been investigated by several researchers. Zhang[17] investigated the strength and durability characteristics of the fine iron tailing sand stabilized by the alkali–activated material, which is used for the construction of the pavement base. It was found that the alkali–activated stabilizer demonstrated a better stabilization capability than the cement for the improvement of the strength and durability of the soil. Abdullah et al.[18] found that the addition of the fly ash–based geopolymer could improve the durability performance of the stabilized clay. The degradation in the integrity and durability of the stabilized clay was mainly attributed to the compromise of the geopolymer hydration products during the wet–dry cycles. Baldovino et al.[19] concluded that both the accumulated mass loss of the blends and the split tensile strength of the stabilized soil by the geopolymer were dependent on the porosity/ cement index η / G_{iv}. Consoli et al.[20] and Xiao and Taeseo[21] proposed the predictive models for the unconfined compression strength of the geopolymer stabilized soil, which was correlated with the index η / G_{iv}. However, most existing models for predicting the durability deterioration were used for evaluating the loss of the stabilized soil mass during the wet–dry cycles. The model for predicting the strength deterioration of the stabilized soils due to the wet–dry cycles has not been developed yet in the literature.

The steel slag, the fly ash and the cement were used as the precursor of geopolymer, which was used to loess stabilization. The effect of the wet–dry cycles on the shear strength of the stabilized loess was investigated by the triaxial compression tests. The predictive model for the strength deterioration of the stabilized loess subjected to the wet–dry cycles was proposed by introducing the ratio of the porosity to the GP volumetric fraction, η / G_{v}. In addition, the X-ray diffraction (XRD), the scanning electron microscopy (SEM), and the mercury intrusion porosimetry (MIP) were conducted on the untreated loess and the stabilized loess. It provides the mineralogy and microstructure insight into the stabilization mechanism of the geopolymer and the deterioration characteristics of the stabilized loess.

2 Material and method

2.1 Material

The loess used in this study was obtained from a construction site in Xi'an, China. The sample was collected in a disturbed state by excavation at the depth of around 4 m below the ground level. The soil was oven-dried, crushed and then passed through No. 10 sieve (2.0 mm). Fig. 1 shows the particle size distribution curves of loess. As shown in Table 1, the basic physical properties of the loess were obtained by experimental studies according to *Test Method of Soil for Highway Engineering* (JTG E40–2007)[22].

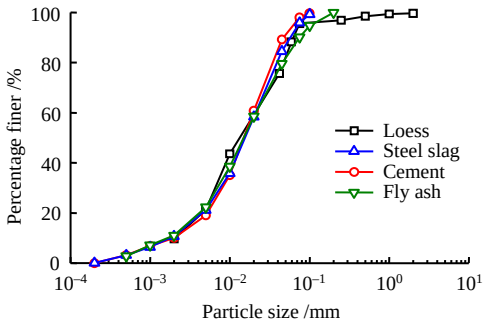

Fig. 1 Particle size distribution curves of loess, steel slag, cement, and fly ash

The steel slag, Grade I fly ash and Portland cement were used as precursor of the geopolymer. The particle size distributions of the untreated loess, the steel slag, the fly ash, and the cement are shown in Fig. 1. The chemical compositions of those raw materials are given in Table 2. The raw material was prepared by mixing steel slag, fly ash, cement and water in a ratio

of 4:4:2:5 by weight. The sodium hydroxide (NaOH) solution with the concentration of 10 mol/L was prepared and used as the alkali activator. The geopolymer was prepared by mixing the raw material mixture and NaOH solution in a ratio of 3:1 by volume (i.e. the ratio of water to raw material by mass is 0.7).

Table 1 Basic physical properties of loess

Plastic limit /%	Liquid limit /%	Plastic index	Clay fraction /%	Silt fraction /%	Sand fraction /%
19.2	32.1	12.9	21.4	74.2	4.4

Table 2 Chemical compositions of raw materials

Raw material	Percentage by weight of chemical compositions /%								
	SiO_2	Fe_2O_3	CaO	Al_2O_3	MgO	K_2O	SO_3	Na_2O	Loss of ignition
Steel slag	31.20	35.40	8.40	9.00	2.40	2.30	3.10	2.74	5.46
Fly ash	52.34	9.62	5.00	24.48	1.91	2.27	0.46	0.78	3.14
Cement	19.40	3.32	60.6	6.84	2.68	0.95	5.26	0.20	0.75

Figure 2 shows the X-ray diffraction (XRD) test result of the geopolymer at the curing time of 28 days. It indicates that the main hydration products include calcium-silicate-hydrate (C-S-H), calcium-aluminosilicate-hydrate (C-A-S-H), calcium hydroxide ($Ca(OH)_2$) and ettringite. Due to the high content of silicon aluminum vitreum, cementitious materials such as C(-A)-S-H were produced in the fly ash and steel slag when exposed to the alkali activator (i.e. NaOH solution). The broadened XRD peak appears at the angle 2θ of 25°–35°, which indicates that the produced geopolymer gel is mainly composed of amorphous minerals[23].

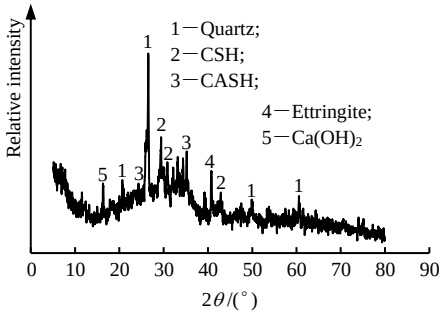

Fig. 2 XRD pattern of geopolymer (GP) at curing time of 28 d

2.2 Specimen preparation

The compacted specimens were used in this study. The geopolymer (GP) contents were 0%, 5%, 10% and 15% by dry weight of the loess. The compaction curves of the untreated loess and the stabilized loess with varied GP contents are presented in Fig. 3. The optimum moisture contents and maximum dry densities of the untreated loess and the GP stabilized loess are given in Table 3. The wet mixing method was used to prepare the stabilized loess specimens by mixing the geopolymer, loess and water. The required water mass to prepare the specimen includes both the added water and the water in the geopolymer at the state of a flowing slurry. The water was added and mixed thorough with the premixed geopolymer and dry loess, such that the optimum water content was reached. Then, the specimens were prepared by compaction in three layers in a cylindrical split steel mold, reaching a specific dry density of 1.8 g/cm^3. The target dry density was used to control the variation of dry density, which will influence the test results. Thus, the result interpretation and the predictive model can be simplified. The cylindrical specimens had a diameter of 39.1 mm and a height of 80 mm. Each specimen was removed from the mold, then was wrapped with plastic film and was finally cured in an environmental chamber at the temperature of 23℃ and the relative humidity of 95% for 28 days.

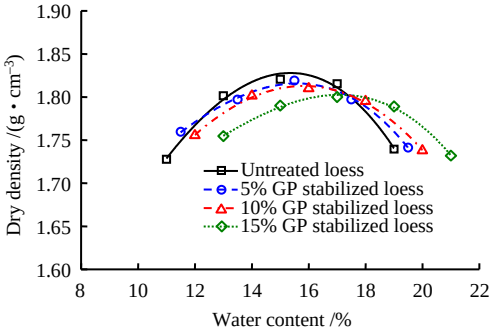

Fig. 3 Compaction curves of untreated loess and stabilized loess with varied GP contents

Table 3 Optimum water contents and maximum dry densities for untreated loess and GP stabilized loess

GP content /%	Optimum water content /%	Maximum dry density /(g • cm^{-3})
0	15.0	1.82
5	15.5	1.82
10	16.0	1.81
15	17.0	1.80

2.3 Experimental program

The wetting followed by drying was used for the wet–dry cycle path. The wetting path was accomplished by spraying water on the surface of specimens which was placed in a cylindrical PVC mold. The water penetration into the specimen lasted for five hours, followed by placing the specimen wrapped with plastic film for one hour and reaching the uniformly distributed water content. The drying path was achieved by oven-drying at the temperature of 40℃ for 24 hours. After the wet–dry cycle number reached 0, 1, 3, 6 and 9, the specimens were wetted to the initial water contents and then submitted to the triaxial compression tests with the confining pressures of 50 kPa, 100 kPa and 150 kPa. The wetting process of the untreated loess was found to be faster than that of the stabilized loess. The remarkable volumetric deformation as well as cracks developed in the untreated loess after multiple wet–dry cycles. The 5% GP stabilized loess developed remarkable volumetric deformation and cracks as well. On the other hand, the 10% and 15% GP stabilized loess underwent insignificant volumetric deformation following wet–dry cycles. The upper bound water contents of the stabilized soils varied after multiple wet-dry cycles due to the deterioration effect; the lower bound water contents of the stabilized

soils are around 12.3% (± 0.1%), which is shown in Fig. 4.

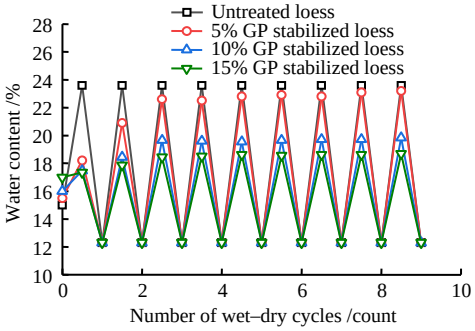

Fig. 4 Wet–dry cycle paths

To investigate the deterioration mechanism of the stabilized loess with varied GP contents from the micro-structure point of view, the scanning electron microscopy (SEM) tests were performed on the stabilized loess specimens after triaxial compression tests. The sub-sized specimens for SEM tests were derived from the cylindrical specimen excluding the shear band and the surrounding damage zone. Multiple positions on the surface of each sub-sized specimen were chosen for SEM observation to ensure the repeatability. Then the SEM images with typical microstructural characteristics were interpreted. In addition, the mercury intrusion porosimetry (MIP) tests were conducted on the specimens after the triaxial compression tests to reveal the pore size distribution of the GP stabilized loess

3 Results and discussion

3.1 Triaxial compression test

3.1.1 Stress–strain curves

Figure 5 presents stress–strain curves of untreated loess and GP stabilized loess (i.e. GP content of 5%, 10% and 15%) under varied confining pressures and wet–dry cycles. It indicates that the peak deviatoric stress decreases as the wet–dry cycle number increases, which demonstrates the deterioration of the untreated loess and the stabilized loess due to the wet–dry cycles. Considering the specimens without any wet–dry cycles, increase of 40% in the peak deviatoric stress from untreated loess to 5% GP stabilized loess was observed. Further increase of GP content to 10% and 15% resulted in peak deviatoric stress increases of 150% and 240%, respectively, than untreated loess. In addition, the stress–strain curves indicate a more remarkable strain-softening and quasi-brittle behavior of the GP stabilized loess when the GP content increases. It is found that the deviatoric stress increases rapidly at the low strain level. This can be attributed to the overconsolidated state of the GP stabilized compacted specimens with a high degree of compaction and dense fabric. As the axial strain increases, the stabilized soil structure destructs, and the deviatoric stress reduces gradually to a stable stress level, i.e. residual strength. For the untreated loess, a deterioration trend in strength was observed from the initial to the third wet–dry cycles, after which a slight strength deterioration and the transition from strain-softening to strain-hardening in the stress–strain behavior took place. For the 5% GP stabilized loess, the strength deteriorates to that of the untreated loess after 9 wet–dry cycles, indicating the destruction of the GP stabilized loess structure due to the accumulative effect of wet–dry cycles. On the other hand, further increase of GP content to 10% and 15% resulted in 75% and 80% of the initial strength, respectively, after 9 wet–dry cycles. It indicates that a less pronounced deterioration effect on the strength of the stabilized loess with a high GP content due to wet–dry cycles. This suggests that a higher GP content results in a more durable structure after the hardening of the GP gel around loess particles, when the stabilized loess undergoes wet–dry cycles.

3.1.2 Cohesion of stabilized loess

Figure 6 shows the dependence of the cohesion of the stabilized loess on the GP content and the wet–dry cycle number. Considering the specimens without any wet–dry cycles, increase of 62%, 176%, and 260% in the cohesion were observed for 5%, 10%, and 15% GP stabilized loess, respectively, than the untreated loess. A remarkable deterioration trend in cohesion was observed in the untreated loess experiencing 3 wet–dry cycles, after which a slight reduction in cohesion took place. For the GP stabilized loess, the cohesion deteriorates in a linear with the number of wet–dry cycles increases. Considering the specimens undergoing 9 wet–dry cycles, the deterioration of 42%, 56%, 30% and 23% in the cohesion for the untreated loess, 5%, 10%, and 15% GP stabilized loess, respectively, were observed. It indicates a more pronounced deterioration effect of the wet–dry cycle on the cohesion of the GP stabilized loess, than the untreated loess. In addition, a higher GP content results in a more durable structure when the stabilized loess undergoes wet–dry cycles.

3.1.3 Internal friction angle of stabilized loess

Figure 7 shows the dependence of the internal friction angle of the stabilized loess on the GP content and the wet–dry cycle number. Considering the specimens without any wet–dry cycles, increases of 6%, 29% and 43% in the internal friction angle were observed for 5%, 10%, and 15% GP stabilized loess, respectively, than the untreated loess. A deterioration trend in internal friction angle was observed in the untreated loess and the GP stabilized loess experiencing 1–3 wet–dry cycles, after which a slight reduction in the internal friction angle occurred. In fact, the variation of the internal friction angle with the wet–dry cycling in the 5% GP stabilized loess is similar to that of the untreated loess. Considering the specimens undergoing 9 wet–dry cycles, the decreases of 3.7%, 9.3%, 8.2% and 7.2% in the internal friction angle for the untreated loess, 5%, 10%, and 15% GP stabilized loess, respectively, were observed. It indicates a less pronounced deterioration effect of the wet–dry cycles on the internal friction angle of the untreated loess and GP stabilized loess than that on the cohesion.

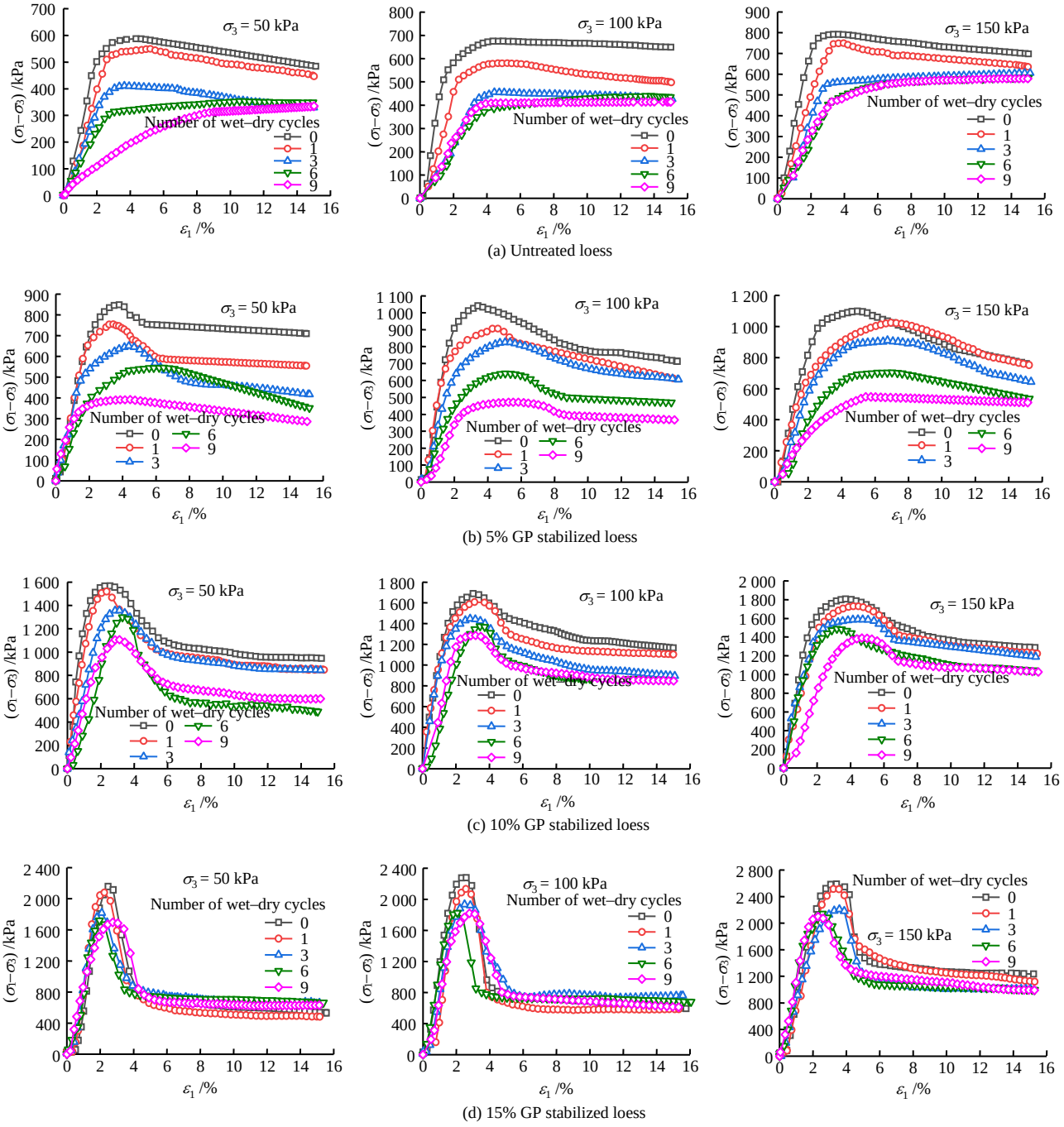

Fig. 5 Stress–strain curves of untreated loess and GP treated loesses under varied confining pressures and GP contents of 5%, 10% and 15%

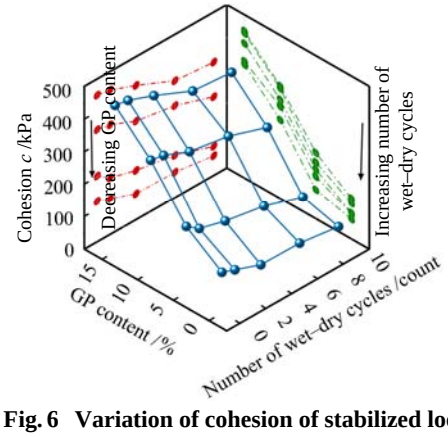

Fig. 6 Variation of cohesion of stabilized loess with GP content and wet–dry cycle number

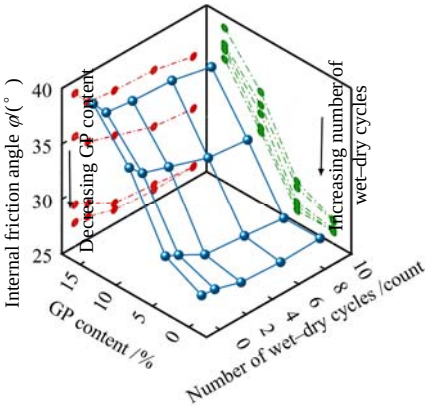

Fig. 7 Variation of internal friction angle of stabilized loess with GP content and wet–dry cycle number

3.2 Prediction model

The triaxial compression test results indicate the pronounced influence of the GP content and the wet–dry cycles on the shear strength of the untreated and GP stabilized loess. Following the approach proposed by Consoli et al.[24], the parameter, i.e. the ratio of the porosity to the GP volumetric fraction (η / G_{v}) is introduced to quantify the influence of GP content on the shear strength of the stabilized loess, such as the peak deviatoric stress $(\sigma_1-\sigma_3)_{\max}$, cohesion c and internal friction angle φ as

$$(\sigma_1-\sigma_3)_{\max}, c, \varphi = A\left(\frac{\eta}{G_{\mathrm{v}}^{x}}\right)^{y} \tag{1}$$

where A is a scalar; x and y are the internal and external power indices.

The calculation results of the parameter η / G_{v} are as shown in Table 4. The formulas for calculating η and G_{v} are given as

$$\eta = 100\% \times \left[1-\frac{\left(\frac{\gamma_{\mathrm{d}}}{1+G/100}\right)}{\gamma_{\mathrm{s}}\gamma_{\mathrm{w}}}-\frac{\left(\frac{\gamma_{\mathrm{d}}}{1+G/100}\right)(G/100)}{\gamma_{\mathrm{G}}\gamma_{\mathrm{w}}}\right] \tag{2}$$

$$G_{\mathrm{v}} = \frac{\left(\frac{\gamma_{\mathrm{d}}}{1+G/100}\right)(G/100)}{\gamma_{\mathrm{G}}\gamma_{\mathrm{w}}} \times 100\% \tag{3}$$

where γ_{d} and γ_{w} are the unit weight of the dry specimen and water; G is the content of the geopolymer; γ_{s} and γ_{G} are the specific gravity of the untreated loess and the geopolymer, which are 2.70 and 2.65, respectively.

Table 4 Calculated η / G_{v} indices of stabilized loess with varied GP contents

GP content /%	η /%	G_{v} /%	η / G_{v}
15	33.17	8.86	3.74
10	33.22	6.17	5.38
5	33.27	3.23	10.30

3.2.1 Deterioration model for peak deviatoric stress

Consoli et al.[25] suggested to take the internal power x as 1 in Eq. (1) for cement stabilized soils. In this study, Eq. (1) combining with x = 1 and y = –0.85 captures the variation of the peak deviatoric stress with respect to the ratio of η / G_{v} for GP stabilized soils. As shown in Fig. 8, Eq. (1) combining with model parameters of y and A is calibrated against the measurements of the peak deviatoric stress of the untreated loess and GP stabilized loess under different confining pressures and numbers of wet–dry cycles. It indicates that the peak deviatoric stress decreases exponentially as the ratio of η / G_{v} increases. In addition, the increase of the GP content results in the reduction of the ratio of η / G_{v} and consequently the increase of the peak deviatoric stress. Considering the internal power x = 1, the scalar A and the external power y varies as the number of wet–dry cycles increases, indicating the influence of the wet–dry cycling on the scalar parameter A and the parameter y associated with the GP content. It suggests the different deterioration mechanisms of the stabilized loess with different GP contents undergoing wet–dry cycles.

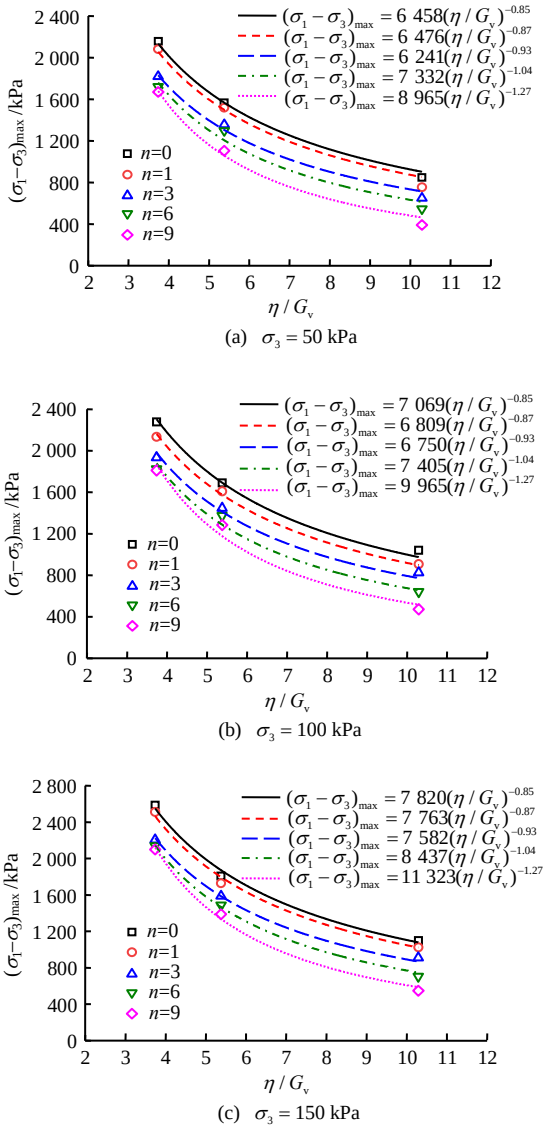

Fig. 8 Variation of peak deviatoric stress of GP stabilized loess with η / G_{v} under varied wet–dry cycle numbers and confining pressures

Based on the calibration results of Eq. (1), it is found that the scalar parameter A varies with the confining pressure and wet–dry cycling. Marques et al.[26] proposed a linear relationship between the parameter A and high confining pressures shearing tests. In this study, the parameter A_0 in the condition of no wet–dry cycles increases linearly with the increasing confining pressure, especially for the low confining pressures (Fig. 9). The linear equation for predicting the parameter A_0 for the stabilized loess with GP content ranging from 5% to 15% under low confining pressures is given as

$$A_0 = 13.62\sigma_3 + 5\,753 \tag{4}$$

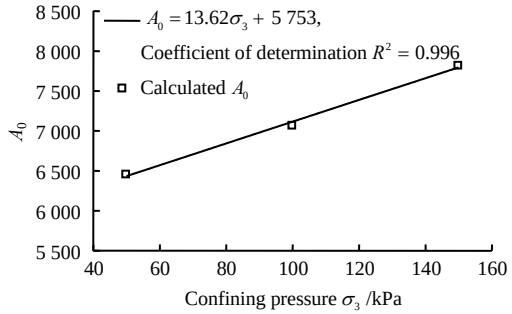

Fig. 9 Variation of scalar A_0 with confining pressure

To account for the influence of wet–dry cycling on the model parameters A and y, the regression analysis for the normalized scalar parameter A_n / A_0 results in

$$A_n / A_0 = 1 - 0.04n + 0.01n^2 \quad (5)$$

where A_0 and A_n are the scalar parameters after zero and n wet–dry cycles; and n is the number of wet–dry cycles.

Figure 10 plots the predicted A_n / A_0 by Eq. (5) against the calibrated results which are dependent on the number of wet–dry cycles. The calibration results of the parameter y is plotted versus the number of wet–dry cycles in Fig. 11, with the regression analysis result as

$$y = -0.85 - 0.01n^{1.72} \quad (6)$$

As shown in Figs. 10 and 11, the remarkable deterioration trend in the peak deviatoric stress of the GP stabilized loess is observed after 3 wet–dry cycles. The change in the GP content results in the variation of the ratio of η / G_v. Consequently, the different deterioration mechanisms in the peak deviatoric stress are detected due to the variation of the ratio of η / G_v and the number of wet–dry cycles, which is consistent with the variation trend as shown in Fig. 5.

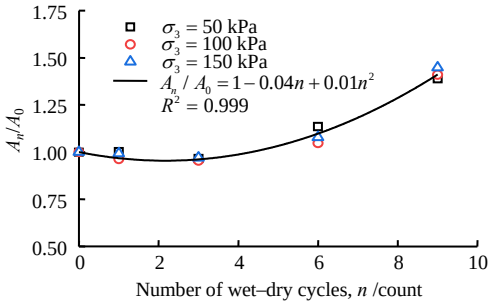

Fig. 10 Variation of A_n/A_0 with number of wet–dry cycles

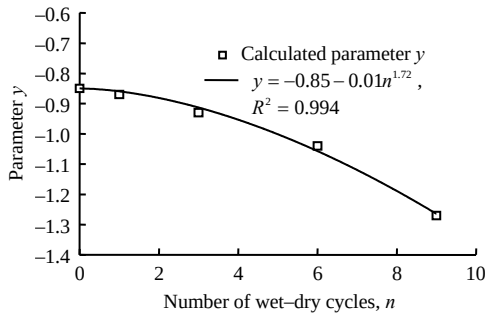

Fig. 11 Variation of parameter y with number of wet–dry cycles

Plugging Eqs. (4), (5) and (6) into Eq. (1) results in the empirical model for predicting the peak deviatoric stress of the GP stabilized loess which deteriorates as the number of wet–dry cycles increases:

$$(\sigma_1 - \sigma_3)_{max} = (13.62\sigma_3 + 5\,753) \cdot (1 - 0.04n + 0.01n^2)\left(\frac{\eta}{G_v}\right)^{-0.85-0.01n^{1.72}} \quad (7)$$

The empirical equation, i.e. Eq. (7) predicts the peak deviatoric stress of the stabilized loess with variable GP contents (i.e. $3.74 \leqslant \eta / G_v \leqslant 10.30$), confining pressures (i.e. 50 kPa$\leqslant \sigma_3 \leqslant$150 kPa), and number of wet–dry cycles (i.e. $0 \leqslant n \leqslant 9$). Fig. 12 plots the predicted peak deviatoric stress by Eq. (7) against the measurements, indicating that the predicted values agree well with the measurements with an error range of ±8%.

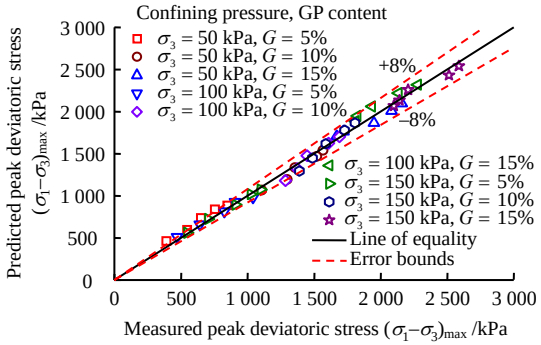

Fig. 12 Comparison of calculated and measured peak deviatoric stresses

3.2.2 Deterioration model for the cohesion

According to the previous studies[27], the similar deterioration trend in the cohesion as the peak deviatoric stress of the stabilized loess subjected to wet–dry cycles was observed. Fig. 13 presents the variation of the cohesion of the stabilized loess with the ratio of η / G_v by Eq. (1) with calibrated model parameters as well as the cohesion derived from the triaxial test results. It indicates that the cohesion of the stabilized loess increases in a power function as the GP content increases, which is similar to the stabilized effect of the cement[28]. The regression analysis of the normalized scalar parameter,

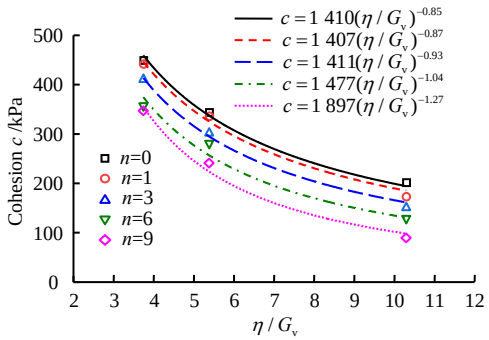

Fig. 13 Variation of cohesion of GP stabilized loess with η / G_v under varied wet–dry cycles

A_n / A_0 for the cohesion of the stabilized loess versus the number of wet–dry cycles n results in

$$A_n / A_0 = 1 + 7 \times 10^{-6} n^{4.9} \quad (8)$$

It gives the similar deterioration trend in the normalized scalar parameter for the cohesion (Eq. (8)) as that for the deviatoric stress (Eq. (5)), which indicates the similar deterioration trend in the cohesion as that in the peak deviatoric stress as the number of wet–dry cycles increases. Substituting Eqs. (6) and (8) into Eq. (1) results in the empirical formula for predicting the cohesion of the GP stabilized loess which deteriorates as the number of wet–dry cycles increases:

$$c = 1\,410(1 + 7 \times 10^{-6} n^{4.9}) \left(\frac{\eta}{G_v} \right)^{-0.85 - 0.01 n^{1.72}} \quad (9)$$

Figure 14 plots the predicted cohesion by the empirical relationship, i.e. Eq. (9) against the measurements, indicating that the predicted values agree well with the measurements with an error range of ±10%. The applicability of Eq. (9) is similar to that of Eq. (7), indicating the similar deterioration trend in the deviatoric stress and the cohesion. Moreover, the deterioration in the shear strength of the stabilized loess subjected to wet–dry cycles is mainly attributed to the reduction in the cohesion.

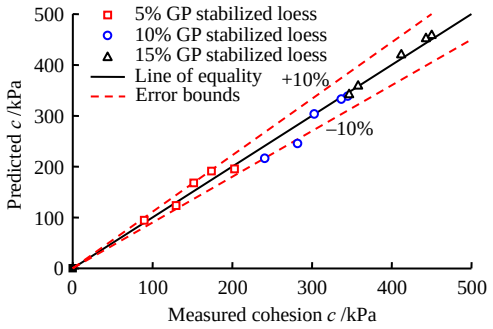

Fig. 14 Comparison of predicted and measured cohesion of GP stabilized loess

3.2.3 Deterioration model of internal friction angle

Figure 15 presents the variation of the internal friction angle of the stabilized loess with the ratio of η / G_v by Eq. (1) with calibrated model parameters as well as the internal friction angle derived from the triaxial test results. It indicates that the internal friction angle of the stabilized loess increases as the GP content increases (Fig. 7), and deteriorates slightly as the number of wet–dry cycles increases (Fig. 15). In addition, it is found that the empirical model (i.e. Eq. (1)) with the external power y = –0.3 can fit well the measurements of the internal friction angle. Thus, the wet–dry cycles has an exclusive effect on the scalar parameter, A in Eq. (1). The variation of the normalized scalar parameter, A_n / A_0 for the internal friction angle of the stabilized loess versus the number of wet–dry cycles, n can be expressed as the best-fit hyperbolic relationship:

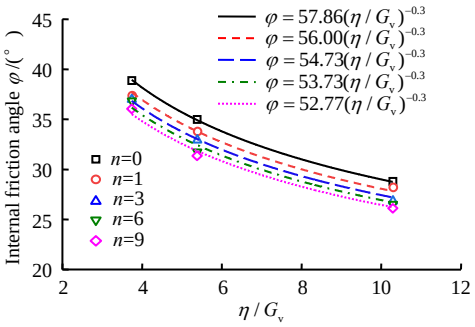

Fig. 15 Variation of internal friction angle of GP stabilized loess with η / G_v under varied wet–dry cycles

$$A_n / A_0 = 1 - \frac{0.038n}{1 + 0.335n} \quad (10)$$

As calculated by Eq. (10), the internal friction angle of the stabilized loess decreases by about 11% after 9 wet–dry cycles, which is consistent with the observations in Fig. 7.

Substituting Eq. (10) into Eq. (1) yields the empirical formula for predicting the internal friction angle of the GP stabilized loess which deteriorates as the number of wet–dry cycles increases:

$$\varphi = 57.86 \left(1 - \frac{0.038n}{1 + 0.335n} \right) \left(\frac{\eta}{G_v} \right)^{-0.3} \quad (11)$$

Figure 16 plots the predicted cohesion by the empirical relationship, i.e. Eq. (11) against the measurements, which validates the reliability of the prediction model with an error range of ±2%.

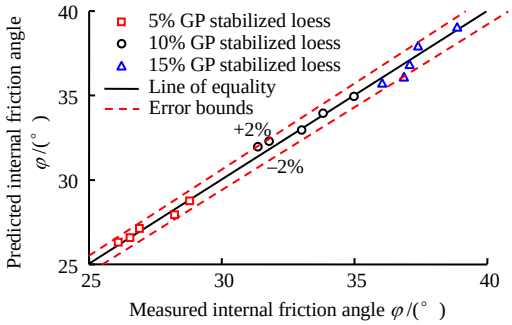

Fig. 16 Comparison of predicted and measured internal friction angle of GP stabilized loess

3.3 Microstructural insight into the deterioration mechanism

3.3.1 SEM observation

Figure 17 presents the SEM images of the GP stabilized loess with different GP contents, i.e. 0, 5%, 10%, 15% without wet–dry cycles and after 9 wet–dry cycles. Considering the specimens before wet–dry cycles, large pores and edge–face contact between particles prevail in the untreated loess; whereas a much denser microstructure and the disperse geopolymer gel (i.e. CSH and CASH) filling the pores between particles

are observed in the GP stabilized loess. The produced short column–shaped ettringite and unreacted spherical fly ash are also detected, which render a compact microstructure to the stabilized loess[29]. After 9 wet–dry cycles, a looser microstructure and a scattered particle arrangement are observed in the untreated loess and the 5% GP stabilized loess. In addition, the connected pores and cracks develop, and the edge–edge contacts between particles become more pronounced. For the 10% GP stabilized loess subjected to wet–dry cycles, the cracks develop and extend in a rather limited range. The appearance of the geopolymer gel (i.e. CSH and CASH) surrounding the crack tips suggests that the binding effect of the geopolymer gel suppresses the development of the cracks and the deterioration of the soil structure. For the 15% GP stabilized loess subjected to wet–dry cycles, the deterioration of soil structure is mainly induced by the destruction of the hardened geopolymer gel. However, the compact microstructure remains, without developing large pores and cracks.

It indicates that the wet–dry cycling results in the irreversible damage in the microstructure of the untreated loess and the stabilized loess with low contents of GP (e.g., 5%). The wet–dry cycles results in the propagation of existing cracks and the initiation of new cracks, which contributes to the deterioration of the soil integrity and homogeneity.

The above microstructure evidences provide insight into the improvement in the durability of the stabilized loess as the GP content increases. The increase of GP content results in the increase of the amorphous geopolymer gel, which fills the soil pores and works as a binder between soil particles. Due to this reason, a more compact microstructure forms and an enhanced shear strength develops in the GP stabilized loess. In addition, the binding effect the geopolymer gel would suppress the development of large pores and cracks, when the stabilized loess deteriorates due to the wet–dry cycles.

3.3.2 Mercury intrusion porosimetry (MIP) results

Figure 18 presents the MIP results, i.e. pore size density of the GP stabilized loess with different GP contents, i.e. 0, 5%, 10%, 15% without wet–dry cycles and after 9 wet–dry cycles. It indicates that the micropores (i.e. 0.01 μm–0.10 μm), small pores (i.e. 0.1–1.0 μm), and intermediate pores (i.e. 1 μm–10 μm) are pronounced in the untreated loess and the 5% GP stabilized loess. The volumetric fraction of the intermediate pores reduces as the GP content increases. After 9 wet–dry cycles, the volumetric fraction of small and intermediate pores increases in the untreated loess and the 5% GP stabilized loess. After 9 wet–dry cycles, the small pores transforms into intermediate pores and large pores (i.e. 10–100 μm) develop in the 10% GP stabilized loess; whereas a less pronounced deterioration effect on the soil structure and no remarkable change in the pore size density are observed in the 15% GP stabilized loess.

It indicates that the intermediate pores in the untreated loess transforms into the micropores and small pores after filling the geopolymer gel, which renders a more compact microstructure in the GP stabilized loess. Considering the stabilized loess with a low GP content subjected wet–dry cycles, the loss of soil particles and the geopolymer gel results in the increase of the micropores and small pores, part of which transforms into intermediate and large pores. On the other hand, no remarkable evolution of the microstructure is observed in the 15% GP stabilized loess subjected to wet–dry cycles. It can be concluded that the pore size density is a remarkable indicator for the structure deterioration of the GP stabilized loess subjected to wet–dry cycles. The microstructure evidences justify the reliability of the deterioration model for predicting the shear strength of the GP stabilized loess subjected to wet–dry cycles as well.

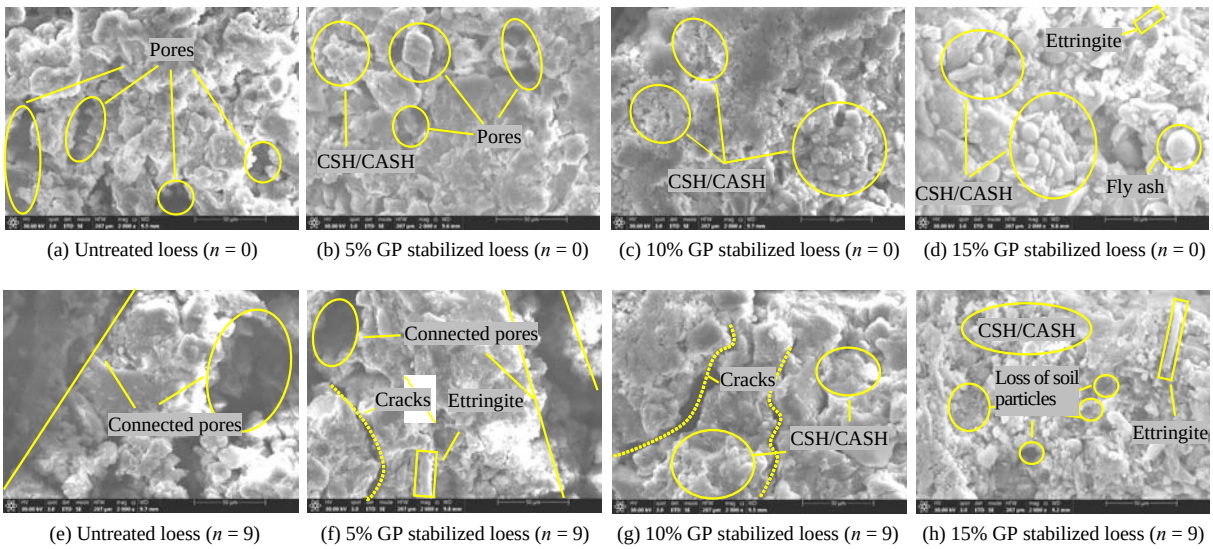

(a) Untreated loess (n = 0) (b) 5% GP stabilized loess (n = 0) (c) 10% GP stabilized loess (n = 0) (d) 15% GP stabilized loess (n = 0)

(e) Untreated loess (n = 9) (f) 5% GP stabilized loess (n = 9) (g) 10% GP stabilized loess (n = 9) (h) 15% GP stabilized loess (n = 9)

Fig. 17 SEM images of stabilized loess with varied GP contents and wet–dry cycle numbers

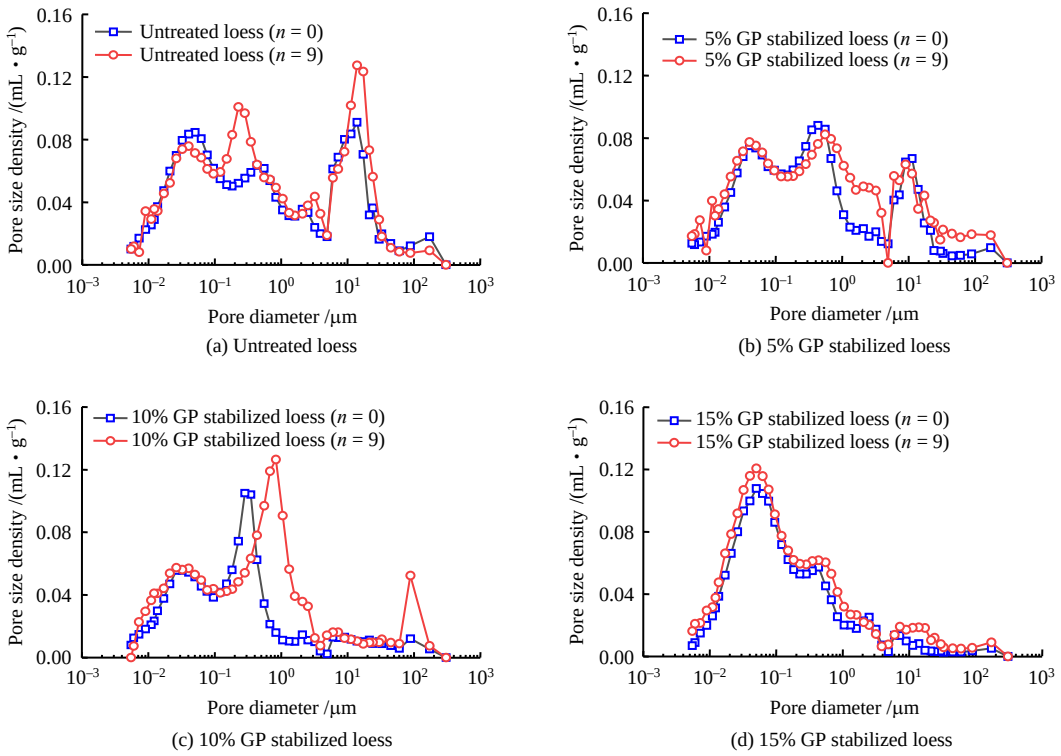

Fig. 18 Pore size distribution of stabilized loess with varied GP contents and wet–dry cycle numbers

4 Conclusions

The strength deterioration of the geopolymer stabilized loess due to the wet–dry cycles was investigated by the triaxial compression tests. The empirical models for predicting the shear strength of the stabilized loess were proposed, which consider the influence of the GP content, the number of wet–dry cycles and the confining pressure. Moreover, the information on the microstructure evolution provided insight into the deterioration mechanism of the strength of the stabilized loess subjected to the wet–dry cycles. The main conclusions are drawn as follows:

(1) The addition of geopolymer could significantly improve the shear strength of the loess. The strength increased as a negative power function with the increase of the ratio of the porosity to the GP volumetric fraction, η / G_{v}. The increase of 260% and 43% were observed in the cohesion and the internal friction angle, respectively in the 15% GP stabilized loess. The strain-softening behavior was detected in the triaxial stress–strain curves of the untreated loess. The brittleness became more pronounced as the GP content increases in the stabilized loess.

(2) The wet–dry cycling resulted in the strength deterioration of the untreated loess and stabilized loess. The deterioration effect of wet–dry cycling on the cohesion was more pronounced than the internal friction angle. As the GP content increased, the durability performance was improved when the stabilized loess underwent wet–dry cycles. Considering the 5% GP stabilized loess, the strength deteriorated after 9 wet–dry cycles and had the strength near the untreated loess, indicating the deterioration effect offset the durability improvement due to the addition of 5% geopolymer.

(3) The empirical model was proposed for predicting the shear strength of the stabilized loess considering the influences of the GP content, the confining pressure and the number of wet–dry cycles. It was found that the increase of the GP content resulted in the reduction in the ratio of η / G_{v}, with which the peak deviatoric stress, the cohesion and the internal friction angle increased in a negative power function. The model proved to be capable of predicting the strength deteriora- tion of the GP stabilized loess with a limited error range.

(4) The gel, i.e. CSH, CASH, etc. were the main hydration products of the geopolymer. The increase of the addition of the GP content led to the increase of the geopolymer gel, which filled the soil pores and worked as a binder between particles. Due to this reason, a more compact microstructure was observed, which rendered the improvement of the durability of the microstructure and macroscopic shear strength of the GP stabilized loess. Considering the untreated loess and the stabilized loess with a low GP content (i.e. 5% and 10%), the wet–dry cycling gave rise to the damage to the microstructure, and the micropores and small pores were enlarged and transformed into the intermediate and large pores. For the stabilized loess with a high GP content (i.e. 15%), the strength deterioration was mainly attributed to the destruction of the geopolymer gel.

References

[1] LIU Song-yu, DU Guang-yin, MAO Zhong-liang, et al. Field tests on improvement of collapsible loess by

vibratory probe compaction method[J]. Chinese Journal of Geotechnical Engineering, 2020, 42(8): 1377−1383.

[2] JIANG Ying-jun, WANG Han-yue, QIAO Huai-yu, et al. Stability of cement-modified loess subgrade under water, wet-dry and freezing-thawing cycles[J]. Science Technology and Engineering, 2020, 20(35): 14592−14599.

[3] ZHONG Xiu-mei, WANG Qian, LIU Zhao-zhao, et al. Dynamic strength of fly ash-modified loess subgrade under influences of drying-wetting cycle[J]. Chinese Journal of Geotechnical Engineering, 2020, 42(Suppl.1): 95−99.

[4] JI Hui, ZHANG Tao, LIU Bao-jian, et al. Experimental study on shear mechanical properties of compound improved loess under wet and dry cycle[J]. Journal of Yangtze River Scientific Research Institute, 2021, 38(8): 120−126, 132.

[5] PRUD'HOMME E, MICHAUD P, JOUSSEIN E, et al. In situ inorganic foams prepared from various clays at low temperature[J]. Applied Clay Science, 2011, 51(1−2): 15−22.

[6] ZHOU Heng-yu, WANG Xiu-shan, HU Xing-xing, et al. Influencing factors and mechanism analysis of strength development of geopolymer stabilized sludge[J]. Rock and Soil Mechanics, 2021, 42(8): 2089−2098.

[7] TAN Yun-zhi, KE Rui, CHEN Jun-lian, et al. Enhancing durability of lime-cement solidified sludge with metakaolin[J]. Rock and Soil Mechanics, 2020, 41(4): 1146−1152.

[8] ZHANG Shu-zheng, GONG Ke-cheng. Geopolymer[J]. Journal of Materials Science & Engineering, 2003, 21(3): 430−436.

[9] LIU Z, CAI C S, LIU F Y, et al. Feasibility study of loess stabilization with fly ash-based geopolymer[J]. Journal of Materials in Civil Engineering, 2016, 28(5): 04016003.

[10] CRISTELO N, GLENDINNING S, PINTO A T. Deep soft soil improvement by alkaline activation[J]. Proceedings of the Institution of Civil Engineers-Ground Improvement, 2011, 164(2): 73−82.

[11] CRISTELO N, GLENDINNING S, MIRANDA T, et al. Soil stabilization using alkaline activation of fly ash for self compacting rammed earth construction[J]. Construction and Building Materials, 2012, 36: 727−735.

[12] CRISTELO N, GLENDINNING S, FERNANDES L, et al. Effect of calcium content on soil stabilization with alkaline activation[J]. Construction and Building Materials, 2012, 29: 167−174.

[13] CRISTELO N, GLENDINNING S, FERNANDES L, et al. Effects of alkaline-activated fly ash and Portland cement on soft soil stabilization[J]. Acta Geotechnica, 2013, 8(4): 395−405.

[14] QIAO Zi-qin. Study on strength characteristics and influencing factors of industrial residue composite solidified loess[D]. Lanzhou: Lanzhou University, 2018.

[15] DENG Yong-feng, ZHAO Yu, LIU Qian-wen, et al. Na_2SiO_4- and cement- based activation on steel slag and its application in soft-soil stabilization[J]. China Journal of Highway and Transport, 2018, 31(11): 11−20.

[16] WU Jun, ZHENG Xi-yao, YANG Ai-wu, et al. Experimental study on the compressive strength of muddy clay solidified by the one-part slag-fly ash based geopolymer[J]. Rock and Soil Mechanics, 2021, 42(3): 647−655.

[17] ZHANG Zhi. Study on strength characteristics and durability of alkali-excited materials modified fine iron tailings sand for pavement base[D]. Fuxin: Liaoning University of Engineering and Technology, 2019.

[18] ABDULLAH H H, SHAHIN M, WALSKE M, et al. Systematic approach to assessing the applicability of fly-ash-based geopolymer for clay stabilization[J]. Canadian Geotechnical Journal, 2020, 57: 1356−1368.

[19] BALDOVINO J D J A, IZZO R D S, ROSE J L, et al. Geopolymers based on recycled glass powder for soil stabilization[J]. Geotechnical and Geological Engineering, 2020, 38(4):4013−4031.

[20] CONSOLI N C, MORALES D P, SALDANHA R B. A new approach for stabilization of lateritic soil with Portland cement and sand: strength and durability[J]. Acta Geotechnica, 2021, 16(5): 1473−86.

[21] XIAO W, TAESEO K. New design chart for geotechnical ground improvement: characterizing cement-stabilized sand[J]. Acta Geotechnica, 2020, 15(3): 999−1011.

[22] China Academy of Transportation Sciences. JTG E40—2007 Test methods of soils for highway engineering[S]. Beijing: People's Communications Press, 2007.

[23] JIANG Yong, JIA Lu-jun, WEN Meng-yuan, et al. Preparation of alkali-activated fly ash/steel slag cementitious materials[J]. Bulletin of the Chinese Ceramic Society, 2019, 38(7): 2152−2156, 2161.

[24] CONSOLI N C, FOPPA D, FESTUGATO L, et al. Key parameters for strength control of artificially cemented soils[J]. Journal of Geotechnical and Geoenvironmental Engineering, 2007, 133(2): 197−205.

[25] CONSOLI N C, MARQUES S F V, FLOSS M F, et al. Broad-spectrum empirical correlation determining tensile and compressive strength of cement-bonded clean granular soils[J]. Journal of Materials in Civil Engineering, 2017, 29(6): 06017004.

[26] MARQUES S F V, FESTUGATO L, CONSOLI N C. Stiffness and strength of an artificially cemented sand cured under stress[J]. Granular Matter, 2021, 23(2).

[27] XU Jian, ZHENG Xiang, WANG Zhang-quan. Investigation for water and salt migrations on spalling disease of loess slope caused by salification erosion[J]. Journal of Engineering Geology, 2018, 26(3): 741−748.

[28] DENG Lin-fei, RUAN Bo. Experimental study on triaxial compression test of polypropylene fiber reinforced cement silty clay[J]. Journal of Railway Science and Engineering, 2019, 16(5): 1201−1206.

[29] WANG Dong-xing, WANG Hong-wei, ZOU Lie-wei, et al. Research on micro-mechanisms of dredged sludge solidified with alkali-activated fly ash[J]. Chinese Journal of Rock Mechanics and Engineering, 2019, 38(Suppl.1): 3197−3205.